NIWA

Taihoro Nukurangi

The acoustic response of orange roughy and associated species from numerical models

Gavin Macaulay

Final Research Report for
Ministry of Fisheries Research Project ORH2001/01
Objective 3

National Institute of Water and Atmospheric Research Ltd

20 January 2004

Final Research Report

Report Title	The acoustic response of orange roughy and associated species from numerical models
Author	Gavin Macaulay

1.	**Date**	30 November 2003
2.	**Contractor**	National Institute of Water and Atmospheric Research Limited
3.	**Project Title**	Estimation of abundance of orange roughy in selected areas
4.	**Project Code**	ORH2001/01
5.	**Project Leader**	Ian Doonan

6. Duration of Project

Start date:	1 June 2002
Completion date:	30 November 2003

7. Executive Summary

An anatomically detailed scattering model has been developed that simulates the scattering of acoustic pulses from fish. Estimates of the target strength for orange roughy and seven associated species have been calculated and are in good agreement with existing target strength estimates. The model is now suitable for use with more species, and also for the investigating means of improving the acoustic target identification of fish.

8. Objectives

This report details work carried out under Objective 3 of Project ORH2001/01: To evaluate alternative acoustic techniques for estimating low densities of orange roughy and associated species. The focus was on the development and testing of an anatomically detailed acoustic scattering model of fish, and the realistic simulation of scattering from fish, with the aim of using the model to investigate techniques for acoustic species identification.

9. Introduction

Estimates of abundance are required for the stock assessment of any species. The Deepwater Medium Term Research Plan discusses the need to estimate the abundance of orange roughy in each of the main fisheries on a regular basis.

Acoustic surveys are the preferred method in situations where orange roughy form dense aggregations that constrain the application of other methods (e.g., trawl surveys). However, although acoustic techniques for deepwater fisheries have developed appreciably in recent years, there is uncertainty about whether they can reliably be used when orange roughy are in

low densities and mixed with other species with gas-filled swim bladders with a correspondingly stronger acoustic echo.

Recent survey results from the Northwest Hills and Spawning Box indicate that a high proportion of the biomass is outside the spawning aggregations, and hence measuring fish in lower density areas is important for monitoring the stocks. An important uncertainty in the stock assessments of orange roughy on the Chatham Rise (both Northwest and Northeast stocks) is the scaling up from spawning biomass to the total stock biomass. This ratio and its inter-annual variability, are poorly estimated for the Chatham Rise stocks, being derived largely from trawl surveys of the Mid-east Coast orange roughy stock, and a limited survey in support of the egg production survey of the Northwest Hills in 1996.

To address this problem with acoustic techniques requires better acoustic target identification, with the eventual aim of being able to classify every echo to species and hence to estimate roughy biomass in areas where they do not form monospecific aggregations.

Fisheries acoustic techniques are still under active development particularly in the area of species identification. Techniques that have been widely used in allied fields (e.g., oil exploration, submarine detection) for many years are only now being applied to fish identification. There have been a number of advances recently, including the acoustic identification of orange roughy using rate-of-change-of-phase (Barr et al. 2000) and response to chirps (Barr 2001; Barr & Coombs 2001).

A variety of transmitted signals have been used for target identification in other fields (e.g. see Gjessing 1986), which exploit various physical characteristics of the targets. During past roughy and oreo surveys small amounts of data have been collected using a variety of waveforms but there are problems with target identification and systematically evaluating a wide range of signals in the field.

This report details the development of an anatomically detailed acoustic scattering model that simulates the acoustic response of fish. It is particularly useful for fish without a gas-filled swimbladder, for which swimbladder casts and subsequent modelling is not appropriate. The model is based on the solution, in the time-domain, of the three-dimensional acoustic wave equation, and uses the finite-difference technique. The model is used to estimate the reflected acoustic waves from various species of fish, and also to calculate the target strength of these fish. Where available, these results are then compared to in-situ estimates.

10. Methods

A scattering model of fish has been developed that incorporates detailed data on fish anatomy, and realistically models acoustic scattering from fish. The theoretical basis of the model is presented, followed by the numerical technique used to obtain solutions in the time domain. The methods used to obtain the fish property data are then discussed, followed by the details of the simulation runs.

10.1 Theoretical basis

The propagation of sound waves through a fish and surrounding water were modelled using the equations of motion for a lossless fluid with variable sound speed and density (Pierce 1989);

$$\frac{1}{c^2}\frac{\partial^2 p}{\partial t^2} = \nabla^2 p - \frac{\nabla p \cdot \nabla \rho}{\rho}, \quad (1)$$

where c is sound speed, p acoustic pressure, t time, and ρ density. Sound speed and density vary with space, while the pressure varies with space and time.

10.2 Solution of the equations of motion

A three-dimensional finite-difference time-domain (FDTD) algorithm was used to solve equation 1. The differencing equation used was a centred second-order spatial and temporal derivative scheme. All simulations were run with a Courant-Friedrichs-Levy (CFL) number of 0.25. The FDTD region was surrounded by 50 perfectly matched layers (PML) to prevent reflections from the boundaries of the domain. The formulation of Liu & Tao (1997) was used.

Gas-filled swimbladders were modelled using a pressure-release surface, whereby the pressure on the boundary of the swimbladder was set to zero. This simulated a soft surface and was appropriate for structures such as swimbladders. Consequently, no allowance was made for the density of the gas in the swimbladder – the swimbladder was assumed to contain a vacuum and be perfectly reflecting. This compromise was necessary because the FDTD method requires a number of constraints on the inputs to achieve numerical stability. One of these is that the density and sound speed do not change by more than a factor of about 2.5 between adjacent grid points, and hence it is unable to model the abrupt change in density and sound speed between fish flesh and air.

The model as implemented does not allow for directionally dependent material properties (for example, as found in bone), or for acoustic attenuation. For the frequency range and propagation distances of interest here, attenuation is insignificant. The effect of not modelling directionally dependent material properties is unknown.

10.3 Density and sound speed from CT scans

Computed tomography scans were taken from seven species of fish – details on each fish are given in **Table 1**. Fish marked with an asterisk have been previously reported upon – refer to Macaulay et al. (2002) for further details. For all other fish the CT scanner used was a GE HiSpeed Fx/i located at Masterton Hospital. A scan was taken every 5 mm, with a slice thickness of 5 mm. Exposure was 3 seconds per slice, with a tube voltage of 120 kV and current of 15 mA. The field of view was 296 mm, giving a transverse image resolution of 0.578 mm (the 3rd dimension of the resolution volume is the slice thickness, 5 mm). The ambient temperature of the fish and room was 19.5 °C. A proprietary processing algorithm was used to produce the CT images from the raw x-ray data. The data output from the scanner were one HU (Hounsfield) number for each resolution volume. Conversion from these data to physical density was achieved via

$$\rho = d \times 1.1571 + 990.91,$$

where ρ is the tissue density in kg/m^3 and d the HU number from the scanner. This relationship applies to the particular scanner used and was derived from scans of three objects of known density, and is valid for at least the range $-125 \le d \le 207$, corresponding to densities of 850 to 1233 kg/m^3 and covers most of the soft tissue in the fish. Note that this range does not include the density of the wax-ester filled swimbladder in orange roughy, nor bone, but the calculated linear relationship between HU number and density is expected to be valid for these lower and higher densities (Henson et al. 1987).

Sound speed was calculated using the density to sound speed relationship given by Aroyan (2001). Few detailed measurements of sound speed and density exist for orange roughy. Measurements of sound speed at a range of pressures and temperatures in lipid extracted from orange roughy (McClatchie & Ye 2000) gave a value of 1470 m/s at 12°C and atmospheric pressure. This lies within the range of values obtained using Aroyan's relationship on orange roughy soft tissue. A more precise comparison of these results was not possible because the lipid was obtained from the entire fish and does not represent any identifiable part of an orange roughy. Phleger & Grigor (1990) measured the density of lipids in orange roughy and obtained a value of 903 kg/m^3 at 6 °C, and found the source of the lipid (swimbladder, skin, bone, etc) made little difference to the density. This compares to the range of values obtained from the orange roughy swimbladder from CT scans of 841–899 kg/m^3 at 19.5 °C. The average of fish flesh density given by Shibata (1970) compares well to the average density obtained from the CT scans (1050 kg/m^3 and 1052 kg/m^3 respectively).

As in Aroyan (2001), all points with an HU value in the range 150–300 were given a constant sound speed of 1730 m/s, and all points above 300 were given a sound speed of 3450 m/s and taken to represent bone. In addition, all HU values less than –200 were taken to be air and the sound speed and density were set to that of seawater. This scheme attempts to account for the effect of density blurring in the transition from bone to soft tissue, and soft-tissue to air, and also re-immerses the fish in seawater (if scanned in air).

The CT scan data from each fish were re-sampled using linear interpolation to give a grid spacing of 3.0 mm in each dimension. This was sufficient to model frequencies up to about 50 kHz, with at least 10 grid points per acoustic wavelength.

10.4 Simulations

The fish data were each placed in a computation region that was 30 mm wider and 30 mm longer that the fish and extended for approximately 270 mm above the fish – see (Figure 1). The sound speed and density in this region were set to those of seawater with a salinity of 35.0 ppt, temperature of 6.0 °C and a pressure of 10 MPa (nominally 1000 m), giving a density of 1032 kg/m^3 as calculated from the UNESCO equation of state given by Gill (1982) and sound speed of 1491 m/s, calculated from an algorithm given by Fofonoff & Millard (1983).

The normal component of velocity on the outermost layer of the PML was set to zero, simulating a hard boundary. The absorption in the x-direction in the PML was set to zero except for the PML at the x=0 and x=N ends. This, in conjunction with the hard boundary, allowed plane waves travelling in the x-direction to propagate without attenuation, but still be absorbed once they reached the end of the computational domain. In addition, once the incident plane wave had reached the end of the computational domain, the x-direction absorption in all PML regions was inserted so as to better absorb the x-component of any scattered waves.

It was important to reduce any reflections from the computational region boundaries to levels less than those expected from the fish. Many absorbing boundary conditions available in the literature have reflection coefficients in the range –10 to –40 dB, and for fish with target strengths in the range –30 to –50 dB this causes the echoes from the fish to be contaminated with echoes from the boundaries to the extent that the results are meaningless. PML were the only technique with the ability to absorb sufficient energy to meet this criteria, and only then with a rather high number of layers. Most PML applications achieve adequate absorption with about 10 layers. The alternative approach of increasing the size of the computational domain so that reflections from the boundaries did not interfere with the echoes of interest was impractical because of computer memory requirements.

Pulses of various shapes and frequencies were introduced into the domain, travelling in the positive x-direction. The model was time-stepped until a steady state had been reached – in general the steady state was a pressure of zero throughout the domain, indicating that all of the incident and reflected pulses had reached the absorbing boundaries and been absorbed.

The pressure at a range of points in the domain was recorded. These data were decimated from the FDTD model sample rate of 4.6 MHz to 383.33 kHz using the Matlab `decimate` command (which applies an eighth-order lowpass Chebyshev Type I filter and then resamples the smoothed signal). They were then quadrature demodulated using the Matlab `demod` command (which multiplies the signal by a cosine and sine of the modulation frequency and then applies a fifth-order Butterworth lowpass filter). The final step was to apply a filter to duplicate some of the filtering applied in a real echosounder. In this instance a raised cosine finite impulse response lowpass filter with a cutoff frequency of 3.25 kHz, and transition bandwidth 6 kHz was used. A second case with a cutoff frequency of 10 kHz was also used. The effect of the transmitter and transducer on the transmitted and received pulse was not explicitly modelled, but would be partially accounted for by the last filter in the processing chain.

These operations gave the amplitude and phase of the reflected pulse as a function of time at a specific point near the fish. The backscattered target strength (*TS*) of the fish was then calculated via

$$TS = 20\log_{10}\left(\frac{pr}{p_i}\right),$$

where p is the peak of the demodulated and filtered pressure envelope at range r from the centroid of the fish and p_i the peak of the demodulated and filtered pressure envelope incident upon the fish. Note that this definition of the fish target strength value is not tilt-averaged, but rather an estimate at specific incident and reflection angles. For all of the simulations presented in this report the incident wave direction of travel was perpendicular to a line drawn through the mouth and centre of the tail of the fish. The reflected wave was also sampled at this angle, and hence the target strength estimates presented in this report are dorsal aspect values. The ranges at which the fish echoes were recorded were all about 0.3 m from the fish. This is likely to be close to the near-field of the fish and will contribute some uncertainty to the target strength estimates. However, observation of the development and propagation of the scattered waves indicated that by a range of 0.3 m, the scattering field was reasonably stable in time and was representative of the far-field pattern.

The rate-of-change-of-phase (RCP) as defined by Barr et al. (2000) was also calculated from the fish echoes. A linear regression was performed on the phase data from the fish echoes and the slope of this regression taken as the RCP in degrees per metre. The pulse was defined by the half maximum amplitude points.

10.5 Simulation accuracy

The accuracy of the scattering model was verified with two different types of test cases. The first involved simulations of plane wave propagation through a change in acoustic impedance. The impedance change was angled relative to the direction of propagation of the plane wave. Snell's Law gives theoretical solutions for this configuration. Several different angles were simulated and in all cases the angle of the reflected and refracted waves was within 0.2° of the theoretical. The amplitude of the reflected and refracted pulses was always within 0.5 dB of the theoretical.

The second test case was a fluid-filled sphere immersed in a fluid of different density and sound speed, and is much closer to a fish than the above impedance change. There exists an analytical solution for this situation, albeit for the steady-state response (Anderson 1950). A range of sphere radii were simulated and in all cases the backscattered target strength was within 0.5 dB of the theoretical. The scattered wave field was also compared to the theoretical and the correspondence was good in all cases, albeit with a high order harmonic. However this is removed as part of the filtering process when calculating the fish acoustic responses. Accordingly, the FDTD model was assumed to be capable of accurately representing the scattering from fish.

11. Results

11.1 Biological structure of fish relevant to scattering

The swimbladder of orange roughy, which is filled with a wax-ester (Phleger & Grigor 1990), is the least dense part of an orange roughy (about 875 kg/m^3), and is surrounded by more dense objects (gonads, flesh, bone, etc) and hence can be expected to make a major contribution to the scattering from the fish. In addition, orange roughy have a large ossified head in which the bone density ranges from 1300 to 1550 kg/m^3 (the sound speed is assumed to be constant at 3450 m/s – see Section 10.3). The densest parts of the fish are the otoliths at approximately 3100 kg/m^3, although they are quite small. Part of the eye (possibly the lens) is also relatively dense (1240 kg/m^3). The density and sound speed contrast between these parts of the fish and its flesh can also be expected to make a major contribution to the scattering from the fish.

For fish with a gas-filled swimbladder the major source of acoustic scattering is the impedance change between the gas in the swimbladder and the surrounding fish flesh – all other scattering mechanisms in such fish will generate considerably lower amplitude echoes. The two other fish without gas-filled swimbladders were Baxters lantern dogfish and pale ghost shark. Both contain a relatively large liver, with a density of approximately 850 kg/m^3, which will tend to generate strong echoes.

11.2 Target strength pulses

Almost all of the target strength data collected from species in New Zealand waters have been with acoustic pulses of frequency 38 kHz and 0.32 ms duration. This corresponds to 12 acoustic wavelengths and a length in water of approximately 0.47 m. Accordingly, a pulse with these characteristics has been used as input to scattering simulations from the 11 fish, and the reflected pulses (after filtering as discussed in Section 10.4) are presented in Figure 2. Pulses with the wider filter are given in Figure 3, and, as expected, show more of the detail of the unfiltered signals. However, much of this structure is due to the filtering operations performed on the raw FDTD data and it is unclear as to how much fish information is in these signals.

The target strength of the reflected pulses from each fish was calculated and these are given in Table 2. Included for comparison are target strength estimates from previously published length to target strength relationships. However, these are not directly comparable because the FDTD simulation results are at dorsal aspect whereas the other estimates are tilt averaged. To achieve a tilt-averaged target strength using the current computation arrangement requires running the same simulation multiple times with the fish at different rotation angles. This is currently impractical due to the long computation times involved for each simulation.

For all fish where there are specific target strength estimates the correspondence is reasonable, particularly given the dorsal aspect/tilt averaged difference. Note that for the Spottyfaced rattail and Baxters lantern dogfish the difference is much larger and this is attributed to the use of a generic length to target strength relationship, and illustrates the need to obtain specific estimates for each fish of interest rather than using a generic relationship across fish groupings.

The scattered wave field from a fish without a gas-filled swimbladder, orange roughy, is presented in Figure 4. This shows how the incident wave is retarded as it travels through the wax-ester filled swimbladder, which has a slower sound speed than fish flesh. Figure 5 shows the same fish at a later time in the simulation when the scattered wave has formed. Note how complex the wave field is, particularly since the image is a two-dimensional slice through the three-dimensional scattering field. Note also the regions of low amplitude echoes and also that as the model progresses in time, these regions remain relatively constant in location, and correspond to nulls in a TS-tilt angle relationship.

The scattered wave field from a fish with a gas-filled swimbladder, black oreo, is given in Figure 6 and shows how no sound penetrates into the gas-filled swimbladder. A region of less acoustic energy can also be seen below the swimbladder. Figure 7 shows the same fish at a later time in the simulation. Note again the highly directional nature of the wave field. Note also how the region immediately below the swimbladder now has a similar acoustic energy density as the rest of the fish. This illustrates how objects that have a similar or smaller size than the acoustic wavelength do not create acoustic shadows.

11.3 Rate of change of phase

The rate of change of phase for each fish is given in Table 2. From work carried out by Barr & Coombs (submitted) a wide variation in RCP is to be expected from orange roughy, and a much smaller variation in RCP is expected for fish with gas-filled swimbladders. This pattern is evident in the results in the table. The mechanism that gives rise to the RCP values for orange roughy is related to the absence of a strong scatterer (the gas-filled swimbladder) and

hence similar RCP behaviour would be expected, and is seen, from the two other non-swimbladder bearing fish – Baxters lantern dogfish and pale ghost shark. Overall, the RCP results from the simulations are in agreement with current knowledge about RCP from fish.

11.4 Discussion

Given the development of the model and its application to orange roughy and some selected by-catch species, it is now appropriate to extend the use of the model to more by-catch species (particularly the 'mcytophid' type target which has a target strength similar to orange roughy, but different RCP), and also to pulse types that have the potential to extract more information about the fish. Detection of a gas-filled swimbladder in fish has been achieved in earlier work (Barr & Coombs 2001) and the potential for chirps investigated elsewhere (Barr 2001). Both of these techniques can now be studied in greater detail using the new scattering model.

The need remains to obtain experimental verification of the accuracy of the scattering model results, preferably by comparing acoustic measurements from live fish with a scattering model of the same fish. The species of fish need not be orange roughy, but would preferably be a species that will survive in a tank at sea level and allow acoustic measurements to be taken with ease. This would also allow CT scanning of live fish and allow quantification of the uncertainty in using data from CT scans of dead fish.

The scattering models of the fish detailed in this report are computationally intensive, with the smallest fish requiring 30 hours of computer time, and the largest more than 230 hours. The Monte-Carlo type methods for deriving, for example, fish tilt-angle (Coombs & Barr in press), require the calculation of the acoustic response from many thousands of fish. This is not feasible with the current state of the model and speed of computers. Further development of the model would be required to reduce the computational requirements to a level that would be practical for large-scale simulations. A further improvement would be to calculate the true far-field radiation pattern via a surface integral close to the fish (Aroyan 1996). This would also reduce some of the uncertainty in the simulated target strength results.

12. Conclusions

The conclusions are:

- An anatomically detailed scattering model has been developed that accurately simulates the scattering from several test cases and, it is assumed, fish.
- The scattering model has been applied to eleven fish from seven species.
- The target strength and RCP from a 'standard' in-situ target strength pulse has been calculated for each fish.
- The target strength and RCP values are in good agreement with existing estimates and knowledge.
- The model can now be applied to more species and more fish, and also with other incident pulse types.

13. Publications

None.

14. Data Storage

None.

15. References

Anderson, V.C. (1950). Sound Scattering from a Fluid Sphere. *Journal of the Acoustical Society of America 22(4)*: 426–431.

Aroyan, J.L. (1996). Three-dimensional numerical simulation of biosonar signal emission and reception in the common dolphin. Ph.D. thesis. University of California at Santa Cruz. 184 p.

Aroyan, J.L. (2001). Three-dimensional modeling of hearing in *Delphinus delphis*. *Journal of the Acoustical Society of America 110(6)*: 3305–3318.

Barr, R. (2001). A design study of an acoustic system suitable for differentiating between orange roughy and other New Zealand deep–water species. *Journal of the Acoustical Society of America 109(1)*: 164–178.

Barr, R.; Coombs, R.F. (2001). *In situ* target strength measurements and chirp responses of orange roughy (*Hoplostethus atlanticus*). Final Research Report to the New Zealand Ministry of Fisheries. 45 p.

Barr, R.; Coombs, R.F. (submitted). Target rate of change of phase: A new dimension for fish and plankton target identification. *Journal of the Acoustical Society of America.*

Barr, R.; Coombs, R.F.; Macaulay, G. (2000). "Can we discriminate between different deepwater fishes using a standard acoustics target strength ping?" *In*: Bradley, S. (ed) Presented at the Proceedings of the 10th International Symposium on Acoustic Remote Sensing of the Atmosphere and Oceans and Associated Techniques, Auckland, New Zealand, November/December 2000.

Coombs, R.F.; Barr, R. (in press). Acoustic remote sensing of swimbladder orientation and species mix in the oreo population on the Chatham Rise. *Journal of the Acoustical Society of America.*

Doonan, I.; Bull, B.; Dunford, A.; Coombs, R.; Tracey, D.; Hart, A. (2001). Acoustic estimates of the biomass of orange roughy in the Spawning Box and on the Northeastern and Eastern Hills, Chatham Rise, July 2000. New Zealand Fisheries Assessment Report 2001/70. 31 p.

Doonan, I.J.; Hicks, A.C.; Coombs, R.F.; Hart, A.C.; Tracey, D. (2003). Acoustic estimates of the abundance of orange roughy in the Mid-East Coast fishery, June-July 2001. New Zealand fisheries assessment report 2003/4. 22 p.

Fofonoff, P.; Millard, R.C., Jr (1983). Algorithms for computation of fundamental properties of seawater. UNESCO Technical Papers in Marine Science. 53 p.

Gill, A.E. (1982). Atmosphere-Ocean Dynamics. Academic Press Limited. 622 p.

Gjessing, D.T. (1986). Target adaptive matched illumination radar: principles and applications. *IEEE electromagnetic wave series*. 172 p.

Henson, P.W.; Ackland, T.; Fox, R.A. (1987). Tissue density measurement using CT scanning. *Australasian Physical & Engineering Sciences in Medicine 10(3)*: 162–166.

Liu, Q.-H.; Tao, J. (1997). The perfectly matched layer for acoustic waves in absorptive media. *Journal of the Acoustical Society of America 102(4)*: 2072–2082.

Macaulay, G.J.; Hart, A.; Grimes, P.; Coombs, R.; Barr, R.; Dunford, A. (2002). Estimation of the target strength of oreo and associated species. Final Research Report to the Ministry of Fisheries for Project OEO2000/01A Objective 1. 20 p.

McClatchie, S.; Ye, Z. (2000). Target strength of an oily deep–water fish, orange roughy (*Hoplostethus atlanticus*) II. Modeling. *Journal of the Acoustical Society of America 107(3)*: 1280–1285.

Paul, L.J. (1986). New Zealand Fishes: An Identification Guide. Reed Methuen, Auckland. 184 p.

Phleger, C.F.; Grigor, M.R. (1990). Role of wax esters in determining buoyancy in *Hosplostethus atlanticus* (Beryciformes: Trachichthyidae). *Marine Biology 105*: 229–233.

Pierce, A.D. (1989). Acoustics: An Introduction to Its Physical Principles and Applications. 2nd. Acoustical Society of America, Woodbury, New York. 678 p.

Shibata, K. (1970). Study on Details of Ultrasonic Reflection from Individual Fish. *Bulletin of the Faculty of Fisheries of Nagasaki University 29*: 1–82.

16. Acknowledgements

The author wishes to thank Alan Hart for collecting the specimens and for his assistance in preparing the fish for scanning. Stuart McGregor is thanked for organising the use and operation of the CT scanner at Masterton Hospital. Adam Dunford and Roger Coombs are thanked for their assistance with the details of digital filters.

Table 1: Details on the fish that were CT scanned. All lengths are fork length except for the orange roughy, which are standard length.

Fish code	Species name	Length (cm)	Sex	Stage	Gas-filled Swim-bladder	Weight (g)	Scanned in	Voxel size (mm)
BOE002	Black oreo (*Allocyttus niger*)	31.1	m	1	Yes	550	Air	0.578,0.578,5.0
CKX001	Spottyfaced rattail (*Caelorinchus acanthiger*)	36.5	m	2	Yes	155	Air	0.578,0.578,5.0
CSE001	Serrulate rattail (*Coryphaenoides serrulatus*)	36.1	m	1	Yes	180	Air	0.578,0.578,5.0
ETB001	Baxters lantern dogfish (*Etmopterus baxteri*)	74.2	f	-	No	2 305	Air	0.578,0.578,5.0
GSP001	Pale ghost shark (*Hydrolagus bemisi*)	50.6	f	-	No	800	Air	0.578,0.578,5.0
ORH001*	Orange roughy (*Hoplostethus atlanticus*)	38.0	f	4	No	1 746	Air	0.586, 0.586, 5.0
ORH002*	Ibid	36.2	f	4	No	1 846	Water	0.430, 0.430, 5.0
ORH003*	Ibid	30.1	m	3 or 4	No	818	Water	0.430, 0.430, 5.0
ORH004*	Ibid	33.3	f	2 or 6	No	1 321	Water	0.430, 0.430, 5.0
ORH005	Ibid	18.9	m	1	No	225	Air	0.578,0.578,5.0
TVI001	*Rachonurus villosus*	43.2	m	2	Yes	205	Air	0.578,0.578,5.0

Table 2: Dorsal aspect target strength (TS) and rate of change of phase (RCP) from the simulations, along with any existing target strength estimates and method and source. Note that the existing TS values are tilt-averaged values and are not directly comparable to the simulation estimates.

Fish code	TS (dB re 1 m^2)	Existing TS (dB re 1 m^2)	RCP (degrees/m)	Existing TS Method	Existing TS Source
BOE002	–41.1	–39.3	23	in-situ & Monte-Carlo	Doonan et al., 2003
CKX001	–35.3	–48.0	–9	generic with swimbladder	Doonan et al., 2003
CSE001	–40.9	–39.9	5	swimbladder casts	Macaulay et al., 2002
ETB001	–34.2	–39.6	–237	generic with no swimbladder	Doonan et al., 2003
GSP001	–42.2	–42.9	–33	generic with no swimbladder	Doonan et al., 2003
ORH001	–47.4	–48.8	270	in-situ & ex-situ	Doonan et al., 2001
ORH002	–50.5	–49.2	10	ibid	ibid
ORH003	–48.3	–50.5	26	ibid	ibid
ORH004	–48.9	–49.8	–5	ibid	ibid
ORH005	–53.4	–53.7	91	ibid	ibid
TVI001	–41.3	–46.7	5	generic with swimbladder	Doonan et al., 2003

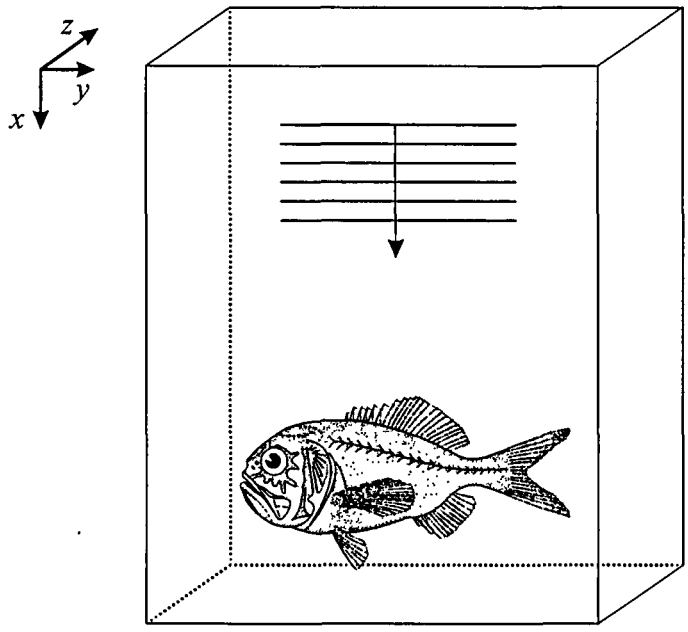

Figure 1. The simulation geometry indicating the location of the fish. The arrow indicates the direction of travel of the incident wave. The six boundary surfaces absorb incident waves using the PML technique. The dimensions of the volume varied to suit the size of the fish. The orange roughy drawing is from Paul (1986).

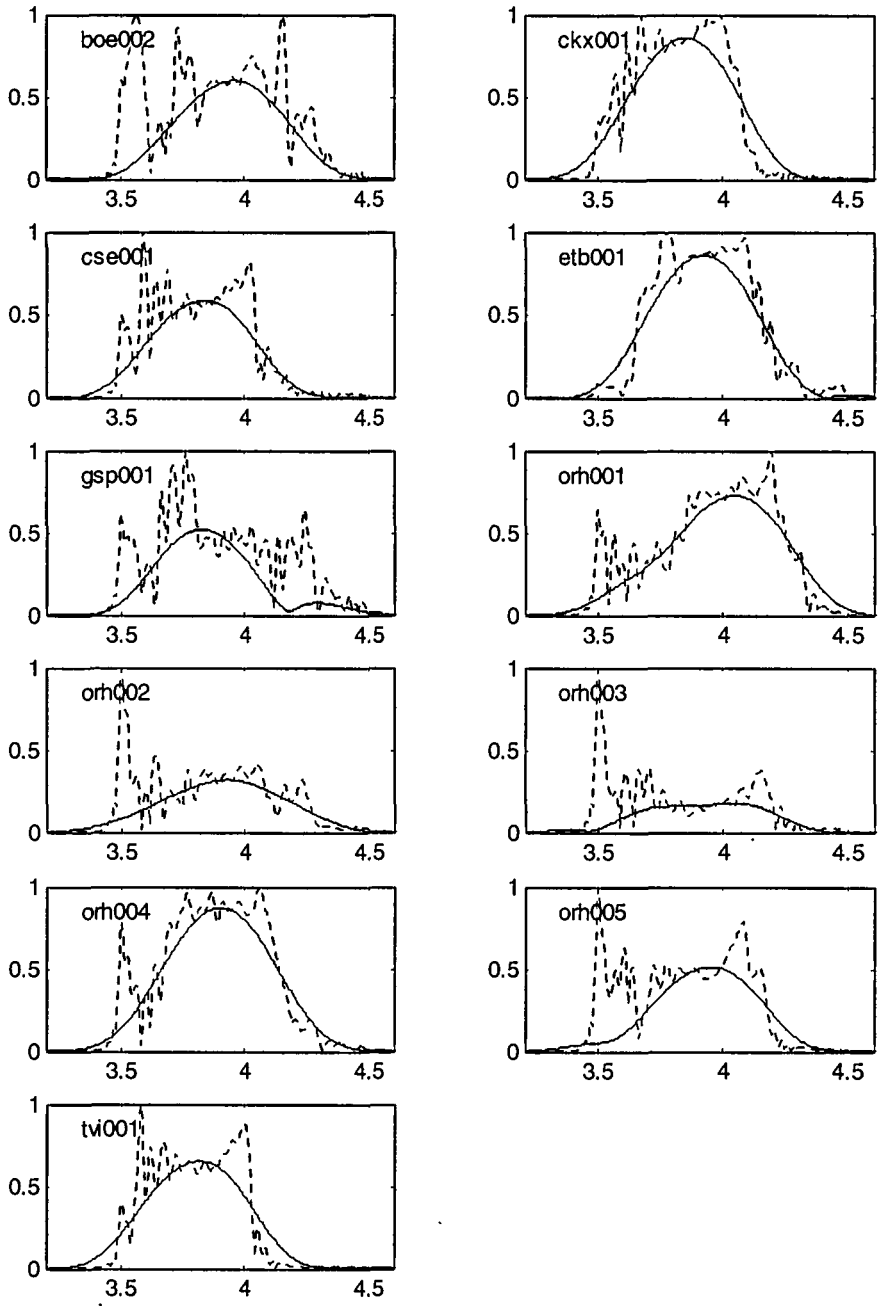

Figure 2: The demodulated pulses from the fish scattering simulations. The y-axis represents pressure in arbitrary units, and the x-axis range in metres, with arbitrary zero. The solid line is the signal after filtering with a low-pass filter with roll-off frequency of 3250 Hz and the dotted line the unfiltered signal.

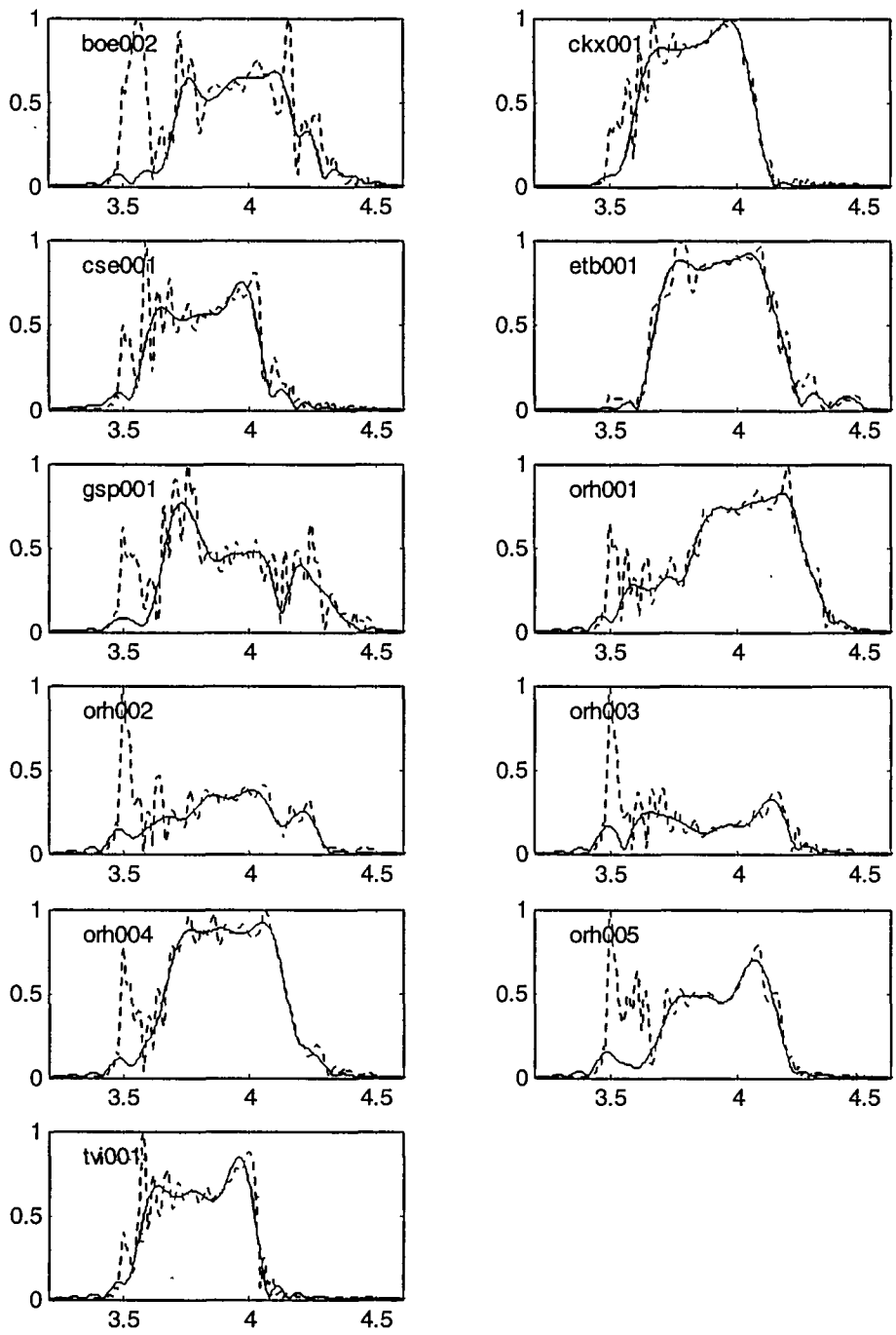

Figure 3: The demodulated pulses from the fish scattering simulations. The y-axis represents pressure in arbitrary units, and the x-axis range in metres, with arbitrary zero. The solid line is the signal after filtering with a low-pass filter with roll-off frequency of 10 kHz and the dotted line the unfiltered signal. Note the enhanced level of detail over the filtered signals presented in Figure 2.

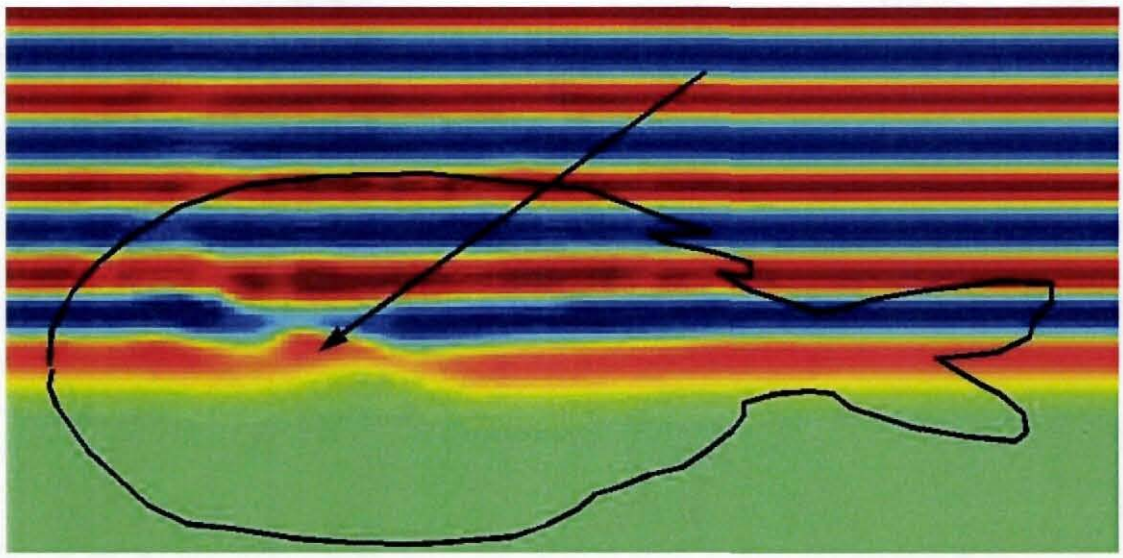

Figure 4: The wave field scattered by fish ORH001 at 24 μs into the simulation. The arrow indicates the retarding of the incident wave by the wax-ester in swimbladder, which has a slower sound speed than in the rest of the fish. A backscattered echo has formed, but is obscured by the much larger incident pulse. The image is a slice midway through the z-axis of the three-dimensional computation volume. The position of the fish is given by the black outline. The colours represent relative acoustic pressure, with blue corresponding to low pressure and red to high.

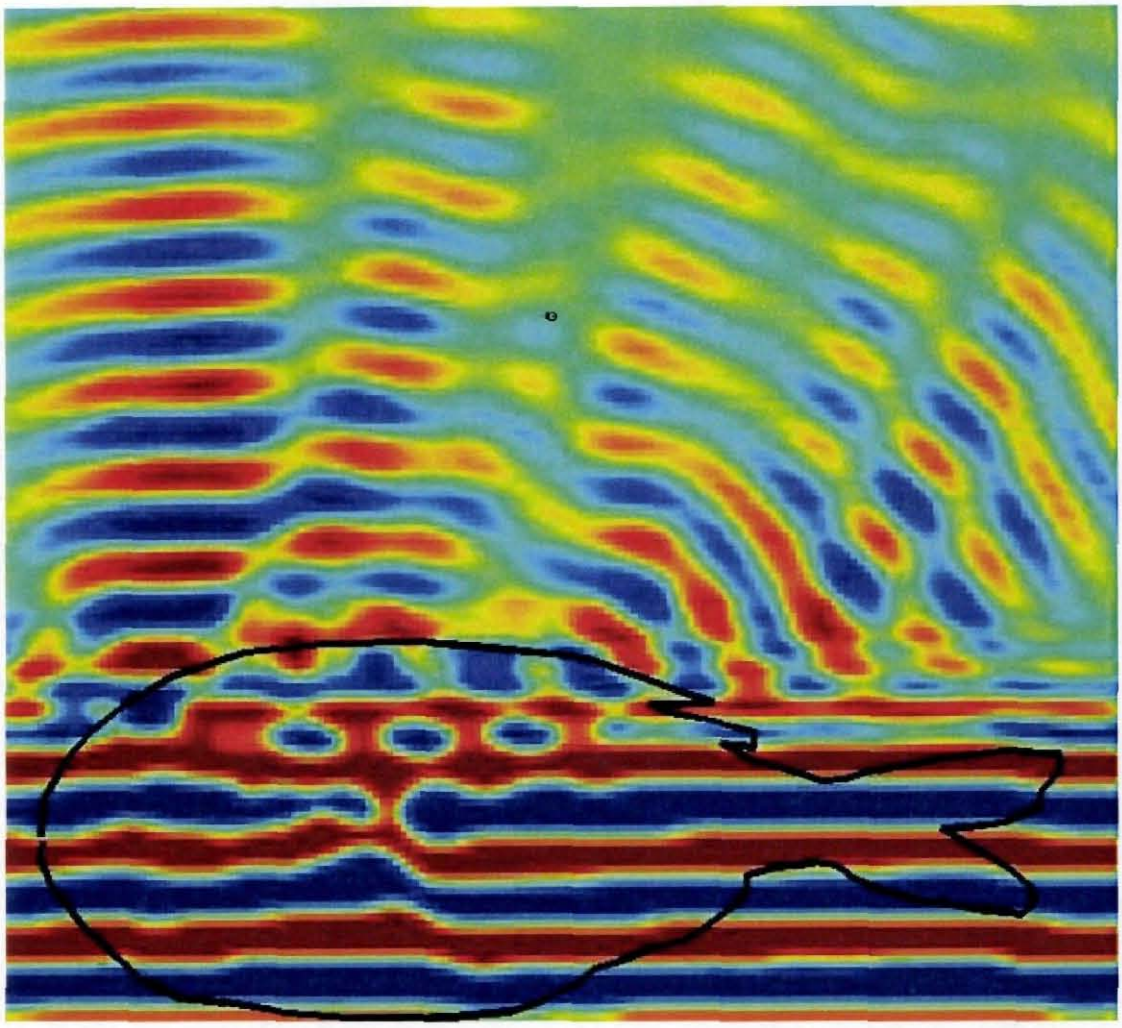

Figure 5: The wave field scattered by fish ORH001 at 54 μs into the simulation. The incident wave has almost passed through the fish and the backscattered echo has formed. The image is a slice midway through the z-axis of the three-dimensional computation volume. The position of the fish is given by the black outline. The colours represent relative acoustic pressure, with blue corresponding to low pressure and red to high.

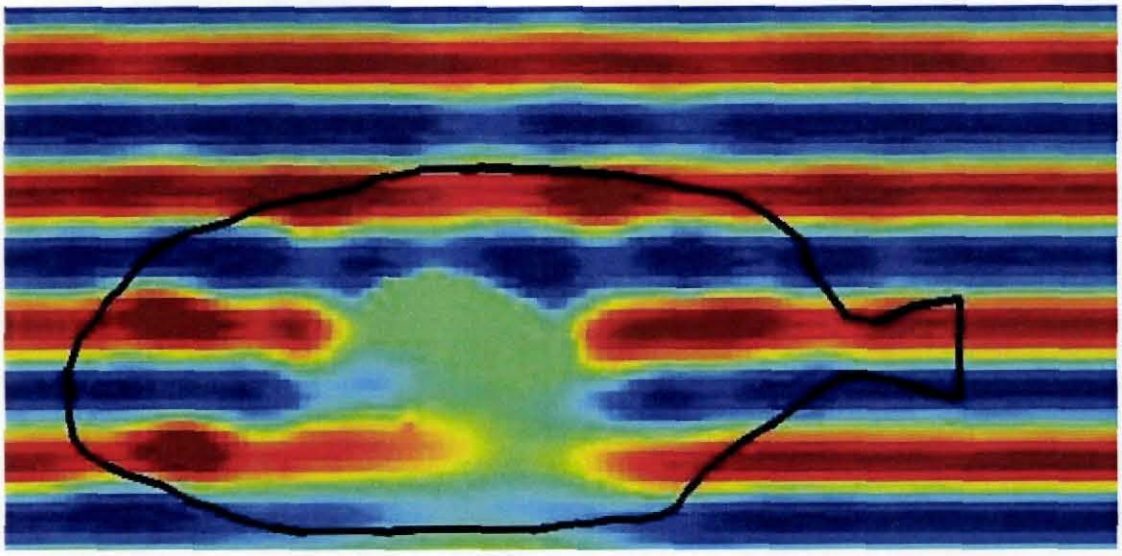

Figure 6: The wave field scattered by fish BOE002 at 29 μs into the simulation. Note the absence of acoustic waves in the gas-filled swimbladder, indicated by the green area in the centre of the fish. The image is a slice midway through the z-axis of the three-dimensional computation *volume. The position of the fish is given by the black outline. The colours represent relative* acoustic pressure, with blue corresponding to low pressure and red to high.

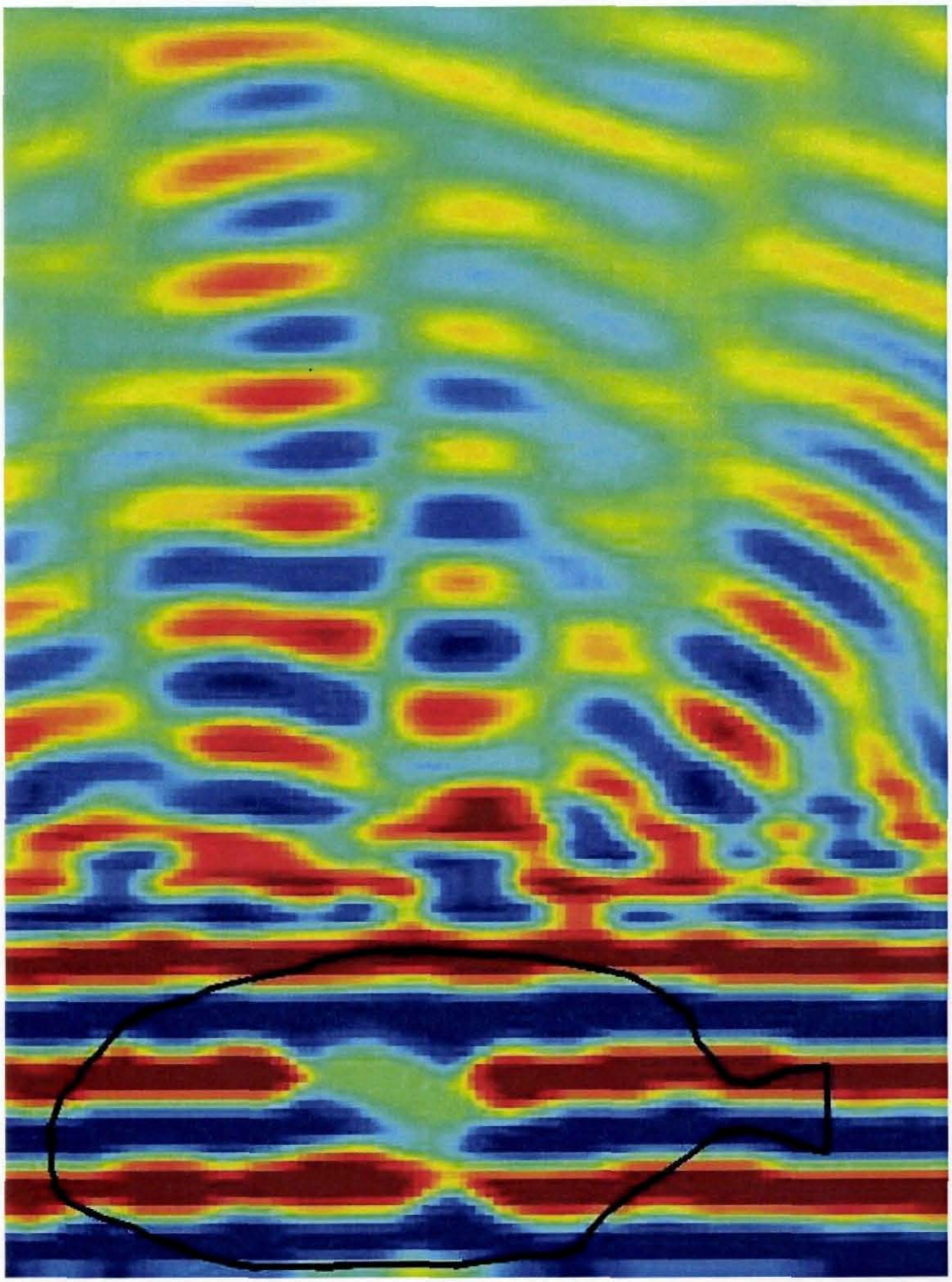

Figure 7: The wave field scattered by fish BOE002 at 52 μs into the simulation. The incident wave has almost passed through the fish and a strongly directional backscattered echo has formed. The image is a slice midway through the z-axis of the three-dimensional computation volume. The position of the fish is given by the black outline. The colours represent relative acoustic pressure, with blue corresponding to low pressure and red to high.